 doi:10.20944/preprints201910.0218.v1

Article

Innovative strategies for bearing lubrication simulations

Franco Concli [1,*], Christian Thomas Schaefer [2] and Christof Bohnert [2]

[1] Free University of Bolzano/Bozen; franco.concli@unibz.it
[2] Schaeffler Technologies AG & Co. KG; christian.schaefer@schaeffler.com, christof.bohnert@schaeffler.com
* Correspondence franco.concli@unibz.it; Tel.: +39-0471-017-748

Abstract: Efficiency improvement is the new challenge in all fields of design. In this scenario the reduction of power losses is becoming more and more a main concern also in the design of power transmissions. Appropriate models to predict power losses are therefore from the earliest stages of the design phase. The aim of the project is to carry on lubrication simulations of several variants of a cylindrical-roller-bearing to understand the lubricant distribution and the related churning power losses. Several strategies to reduce the computational effort have been used. Among them the sectorial symmetry and three innovative meshing strategies (purely analytical with and without interfaces and analytical/subtractive) that have been implemented in the OpenFOAM® environment. The results of the different approaches were compared among them and with experimental observations showing good agreement and reasonable savings in terms of computational effort.

Keywords: bearing; lubrication; CFD; OpenFOAM®; meshing.

1. Introduction

Eco-friendly technologies represent a positive trend for the future. The achievement of ambitious goals in terms of energy savings is strictly related to the capability to design more efficient systems.

In these regards, the recent developments in computer science have opened new possibilities. While in the past different design solutions were characterized from an energetic point of view by means of experimental tests, in the recent years more and more numerical studied are available in literature. Numerical techniques, in fact, allow to overcome the need of prototyping, enabling a comparison and an optimization of the different designs starting from the earliest stages of the development.

With focus on the efficiency/thermal behavior regarding churning of mechanical components, including bearings, CFD (Computational Fluid Dynamic) seems to be one of the most appropriate tools. Among the different approaches, SPH (Smooth Particle Hydrodynamic), a meshless method, has the advantage of being easily applicable [1] even if the accuracy of the results was proved to be insufficient for comparable computational effort [2][3]. On the other side, mesh-based methods such as FV (Finite Volume) ensure a very high accuracy but in most cases the computational effort required is not compatible with the industrial practice [4]. To partially overcome this problem, in the past several attempts were made. In particular, rotating reference frames [5][6], innovative partitioning strategies [7][8] and, mostly, mesh-handling algorithms [9][10][11][12][13] have been developed and applied in order to reduce the simulation effort.

The goal of this research is to study the lubrication and the efficiency of a roller bearing. For this purpose, several levels of geometrical simplifications were introduced. For each model, ad-hoc meshing strategies were developed and implemented in the OpenFOAM® environment. The idea is to try to limit the computational effort by avoiding any kind of mesh deformation and need for

 doi:10.20944/preprints201910.0218.v1

remeshing, together with an analytical control of the mesh generation to better handle the element distribution and quality parameters.

2. Materials and Methods

2.1. Bearing Losses

Bearings allow the relative rotation between two mechanical components. They can be classified into two main categories: journal or rolling bearings.

In journal or hydrodynamic bearings, the converging gap ensures that the two surfaces are kept separated by a fluid film. To the fluid film are associated the supporting lift forces but also the frictional losses. The power dissipation is mainly due to viscous effects. This kind of bearing was already studied in the past by the author using OpenFOAM® [14]. This kind of simulations is relatively simple from a geometrical point of view because the domain doesn't significantly change its shape during operation.

Rolling bearings carry the load by means of interposed rolling elements. Although also in this case a hydrodynamic film generates in the contacts, the predominant interactions for churning losses are due to the rotation of the cage and motion of the rolling elements. This is the main cause both for the lubricant flow and the losses.

The load independent power losses of bearings, in fact, can be classified into seal losses and hydraulic losses. The latter can be further subdivided into squeezing and churning/windage ones.

Squeezing losses are mainly related to volume variations and pressure gradients that causes additional flows. Churning losses are due to the splashing of the lubricant due to the motion of the components. It is well known that the squeezing losses, except for spray lubrication, are of a lower order of magnitude with respect to the churning ones [15][16].

2.2. Bearing Geometry

The bearing considered in this study is a Schaeffler NU222-E-XL-M1/M1A. It is a cylindrical roller bearing which dimensions are listed in table 1.

Table 1. Parameters of the bearing

Dimension	Value	Parameters	Value
d [mm]	110	C_{0r} [kN]	345
D [mm]	200	C_r [kN]	365
B [mm]	38	n_G [rpm]	5300

This model of non-locating bearing with a single row of cylindrical elements has a very high radial load carrying capacity and is suitable for higher speeds compared to full complement designs. The rollers are guided between rigid ribs in the outer ring. The cage has a solid design and is made of brass. The radial clearance is less than 90 μm.

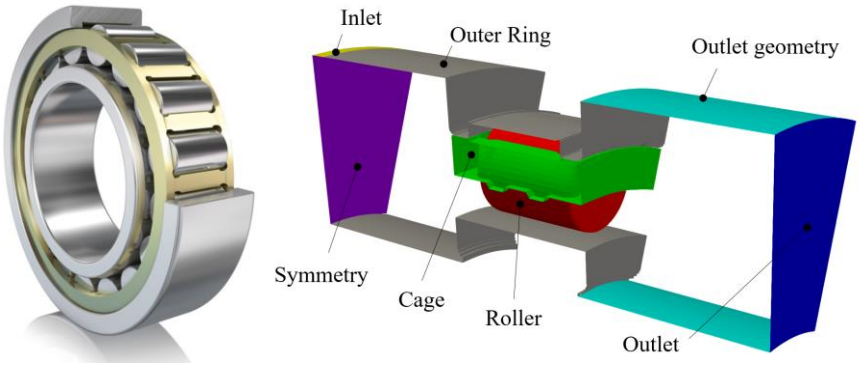

Figure 1. Schaeffler NU222-E-XL-M1A bearing.

Preprints (www.preprints.org) | NOT PEER-REVIEWED | Posted: 18 October 2019 doi:10.20944/preprints201910.0218.v1

The lubricant is supplied radially into the space in front of the bearing. In the studied configuration, the inner ring is rotating with a speed of 4500 rpm (slightly below the limiting speed n_G). The outer ring is steady. Consequently, the rotational speed of the cage results in 1904 rpm and the one of the rollers in 14300 rpm. The lubricant selected for this study is an ISO VG 320 which has, at the simulation temperature of 95°C, a kinematic viscosity of 27.9 cSt (mm^2/s). The density results in 880 kg/m^3.

2.3. Simplifications

The abovementioned bearing model was considered in the study. However, several levels of simplifications have been introduced and studied: presence or not of the outer ring ribs, presence or not of rounding radii, sectorial symmetry (not capable to consider the effect of the gravity). Furthermore, 2 different cages have been analyzed. Table 2 shows the full list of the simulation performed. In simulations #1 to #3, just 1 sector of the bearing (360°/17) was modelled. This was possible thanks to the cyclic symmetry of the system. The study of the effect of the different simplifications was aimed to create a numerical model whose solution requires a limited computational effort.

Table 2. Simulations performed.

Configuration	Bearing	Cage type	Ribs	R. radii	Sectorial/full
#1	NU222-E-XL-M1	M1	no	no	Sect.
#2	NU222-E-XL-M1A	M1A	yes	no	Sect.
#3	NU222-E-XL-M1A	M1A	yes	yes	Sect.
#4	NU222-E-XL-M1A	M1A	yes	yes	Full

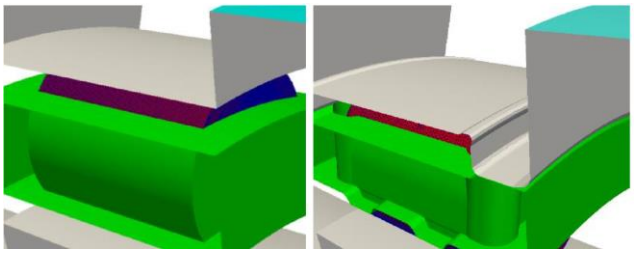

Figure 2. Different configurations: #1 no ribs, no rounding radii, cage M1 (left), #3 ribs, rounding radii, cage M1A (left).

2.4. Meshing strategies

The different configurations have different internal geometries. While the main differences in the topology are due to the presence of the ribs and the cage model, from a meshing point of view, the rounding radii are the most critical parameter to be handled. For this reason, different approaches have been used.

2.4.1. Analytical meshing with interfaces

The "analytical meshing with interfaces" approach was used for simulation #1. A first subdivision of the domain was made axially between the rolling element end faces and the internal face of the cage (whose surface normal is parallel to the bearing axis). A second subdivision was made just after the opposite face of the cage. This was done both for the inlet as well as for the outlet side (purple surfaces in figure 3). This ensures that a mesh with extruded prismatic elements only is created for each axial portion of the domain. The 5 meshes, belonging to the different axial slices of the bearing, result conformal among them from a geometrical point of view, but not conformal in terms of position of the nodes. The introduction of mesh interfaces (AMIs) allows the numerical connection between those meshes. The AMI operates by projecting one of the patches boundary mesh

Preprints (www.preprints.org) | NOT PEER-REVIEWED | Posted: 18 October 2019 doi:10.20944/preprints201910.0218.v1

onto the other ensuring that that the values of a generic field are the same on both sides of the interface.

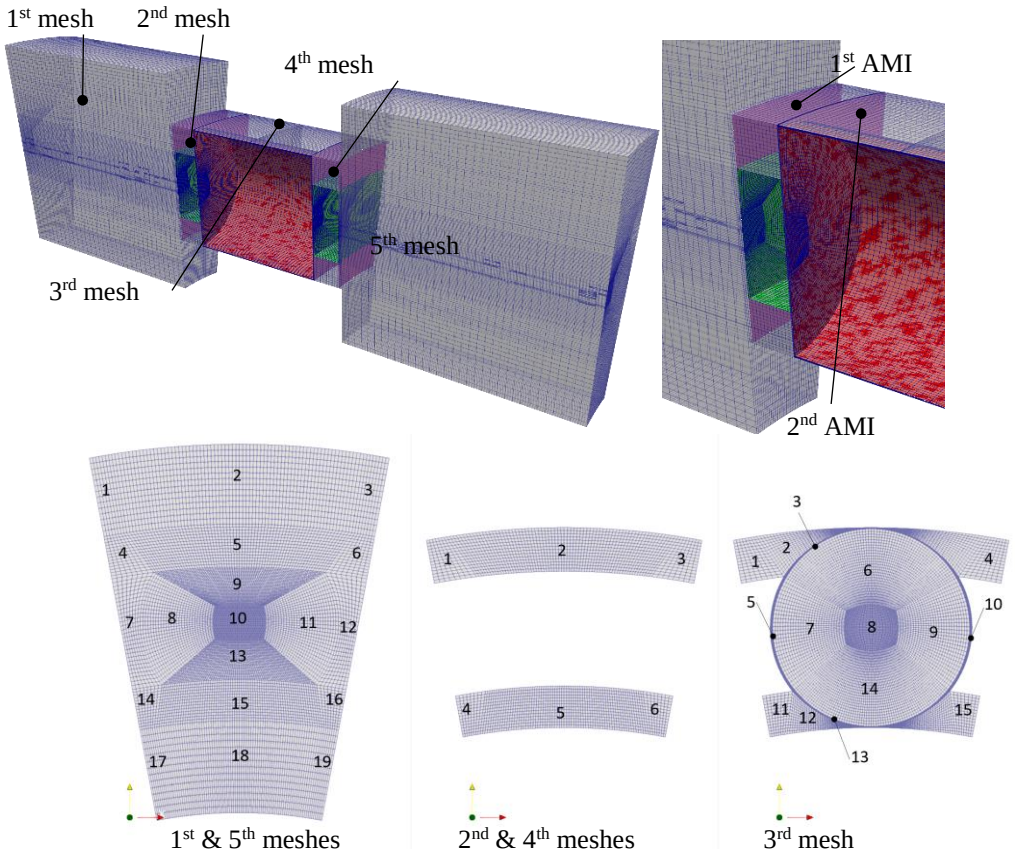

Figure 3. Meshing approach for configuration #1: 4 AMIs are present (purple). In the lower part of the figure the 3 typologies of 2D mesh (successively extruded) are shown.

The principle behind this approach is the decomposition of one lateral face into a set of quadrilaterals. Edges can be straight lines, arcs or splines [17]. The further discretization of the 4 edges polyhedron is defined through the seed of 2 adjacent edges. In figure 3 (bottom left) it can be appreciated that the grid is made of 19 quadrilaterals. The blocks have always 4 edges. Some of them are curved according to a defined function. In block 2 (1st mesh), for example, the upper edge is curved to follow the outer ring curvature. The left edge of block 8 (1st mesh), is curved to follow the curvature of the roller. Other edges (for example of block 10 – 1st mesh) are curved just to keep the quality of the elements above a certain threshold.

The 2nd (and 4th) portion of mesh between the 1st and 2nd AMI (3rd and 4th AMI) (bottom center of figure 3) is made of 6 blocks. The central mesh between the 2nd and 3rd AMIs (bottom right of figure 3) is made of 15 blocks. The possibility to create the mesh as a compound of multiple blocks allows to better control the internal quality of the grid and to significantly speed up its generation. The creation of this grid (1.2M cells) takes, on a 48GFLOPS workstation, only 8 seconds. The finest grid used during the mesh sensitivity analysis with the same block layout, was of about 7.3M cells. Its generation takes about 55 seconds showing a linear scalability.

2.4.2. Analytical meshing without interfaces

For configuration #2, in which the rounding radii were neglected (but not the ribs), it was possible to create the whole geometry with multiple extrusions without the need of AMIs. To achieve this goal, a more complex partition of the frontal (extrusion) surface (figure 4 left) was used. This consists in 39 blocks. Not all the blocks were extruded for the whole bearing length. Block 1 to 5, for example, were missing in the mid (axial) portion where the outer ring is located. In the same way,

Preprints (www.preprints.org) | NOT PEER-REVIEWED | Posted: 18 October 2019 doi:10.20944/preprints201910.0218.v1

blocks 11, 13, 18, 22, 23, 24, 27, 28, 29 and 39 are not extruded in correspondence of the roller. This approach is very powerful and enables the creation of a good quality grid in a very short time (10 s). However, with this approach is not possible to model all the rounding radii like those of the rings and of the roller.

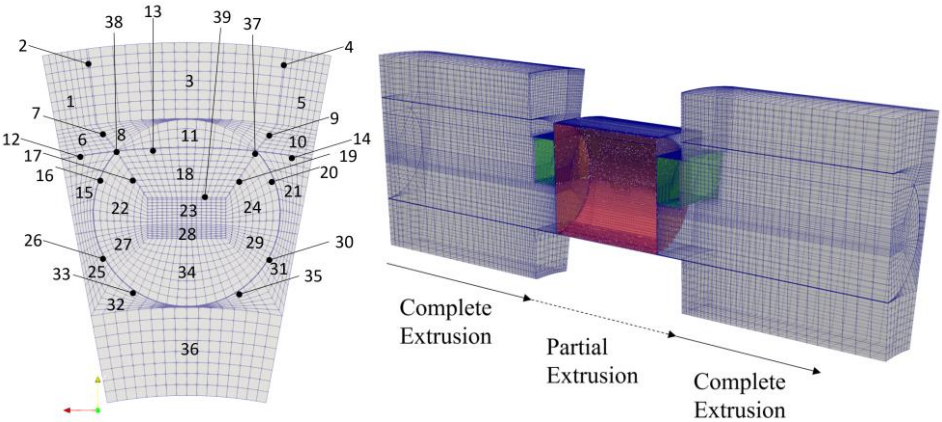

Figure 4. Meshing approach for configuration #2: no AMIs are present. The mesh is generated with a pure analytical approach.

2.4.3. Analytical & subtractive meshing approach

In order to simulate configuration #3, in which all the rounding radii were modelled, a first mesh, without internal cavities (like those corresponding to the roller and the cage for simulation #2) was created analytically with 39 blocks successively extruded. An initial background grid generated (figure 5 up left) in 11 s. Unlike for mesh #2, all the 39 quadrangles where extruded for the whole axial length of the model. Successively, the boundaries corresponding to roller, cage and rings were created with a subtractive approach. In a first stage, the cells that intersect the surfaces of roller, rings and cage (defined via .stl files), were spitted into smaller cells. Each cell is subdivided into 4 smaller cells. Eventually, if required, those cells were further spitted until the desired accuracy is reached. Once this operation is complete, a process of cell removal begins (figure 6).

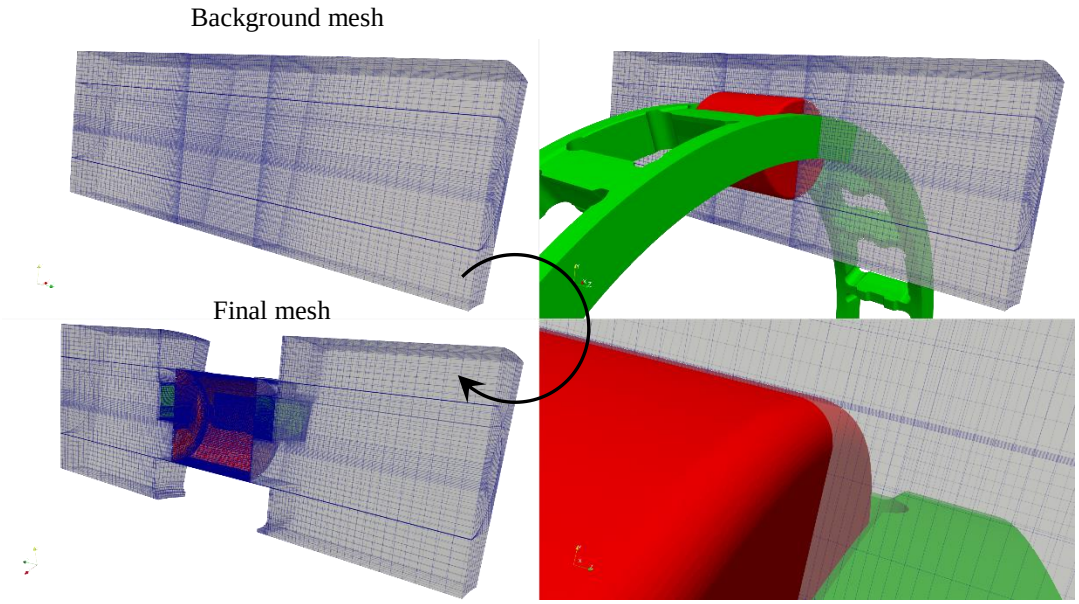

Figure 5. Meshing approach for configuration #3: no AMIs are present. The mesh is generated first a pure analytical approach (up left). Then the cavities corresponding to roller and cage were emptied.

Preprints (www.preprints.org) | NOT PEER-REVIEWED | Posted: 18 October 2019 doi:10.20944/preprints201910.0218.v1

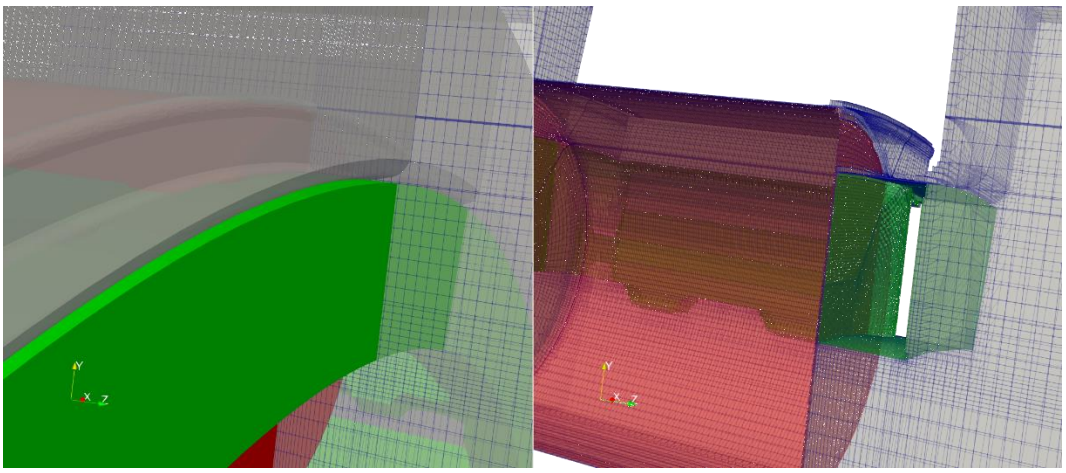

Figure 6. Meshing approach for configuration #3: no AMIs are present. Details of the subtraction: background mesh and .stl files on the left; final mesh after the subtraction on the right.

This approach is very effective but not as efficient as the analytical generation. The conversion of the background grid into the final mesh takes about 75 s. This is in any case a much better results with respect to a comparable automatic tetrahedralization which took, using a Netgen [18] algorithm, about 900 s.

Table 3. Parameters of the meshes

Mesh	#1	#2	#3	#4
points:	1343430	1297328	1035502	17277372
faces:	3832976	3226656	3874220	65442418
cells:	1245328	967904	1442282	24518794

Table 3 summarize the properties of the meshes obtained with the different approaches. The number of cells reduces from configuration #1 to #2 due to the presence, in the latter one, of the ribs that limit the volume of the computational domain. Mesh #3 has the highest number of cells because, to accurately follow the rounding radii, the above described mesh splitting step produces a much finer grid near the boundaries. This is confirmed by a higher number of faces of the grid of configuration #3 that, except for the rounding radii, is very similar to configuration #2.

2.4.4. Full model

To understand the effect of gravity (which relative orientation is a function of the bearing sector position) on the oil flow through and oil distribution in the bearing, , a simulation of the full geometry was also performed. For the rotational speed considered, no significant differences in terms of losses and lubricant distribution are expected with respect to the sectorial model. Nevertheless, to have a complete understanding of the physical phenomena, it is fundamental to investigate also this effect.

To build the full grid, a circular pattern of the sectorial mesh #3 was made. The different meshes are conformal and can be easily stitched together. Therefore, the number of cells of the #4 grid results 17 (number of rollers) times larger with respect to the mesh #3.

Preprints (www.preprints.org) | NOT PEER-REVIEWED | Posted: 18 October 2019 doi:10.20944/preprints201910.0218.v1

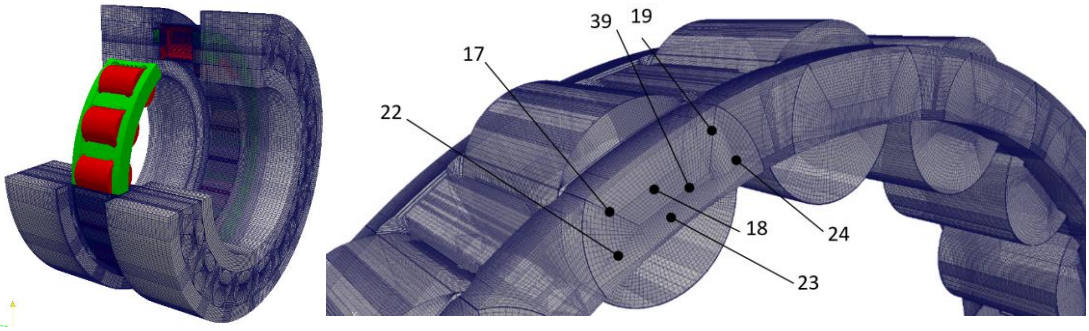

Figure 6. Mesh #4 (groups with reference to figure 4)

2.5. Boundary conditions and mesh motion

A 2-phase incompressible, isothermal solver for immiscible fluids was used. It is based on a VOF (volume of fluid) phase-fraction interface capturing approach. In such applications, in fact, the air flows are as important as the lubricant one and a single-phase simplification is not acceptable. A rigid mesh motion without topology changes or adaptive re-meshing was imposed to simulate the motion of the components. The rotational speed of the grid corresponds to the rotational speed of the cage (1904 rpm). This has required the development of two boundary conditions (B.C.) to properly assign the rotational speed to the different components. Since the grid is rotating, the rotational speed of the rings should be defined in the rotating reference frame by adding (inner ring) or subtracting (outer ring) the proper velocities. In the same way, the roto-translation of the rollers is obtained by adding a pure rotation to the motion of the grid. Table 4 summarizes all the B.C..

Table 4. B.C.

Patch	U [m/s] / ω [rpm]	p [Pa]	α [-]
Roller	ω_z^{rel}=-14300	∇p=0	∇α=0
Outer Ring	ω_z^{rel}=-1904	∇p=0	∇α=0
Inner Ring	ω_z^{rel}=2596	∇p=0	∇α=0
Cage	ω^{rel}=0	∇p=0	∇α=0
Inlet	∇**u**=0	∇p=0	α=1
Outlet	∇**u**=0	p=100000	∇α=0
Outlet geometry	noSlip	∇p=0	∇α=0
Symmetry	symmetry	symmetry	symmetry
Cyclic	cyclic	cyclic	cyclic

Gravity was considered. Simulation were performed limiting the Co number to 1 to ensure numerical stability and good convergence. The solution of the system was performed with a PIMPLE (merged PISO-SIMPLE) algorithm. This conjugates the advantages in terms of computational efficiency of the SIMPLE scheme with the capability of the PISO one to be time-conservative.

Mass, momentum and volume fraction conservation equations were defined as follows:

$$\frac{\partial \rho}{\partial t} + \nabla \cdot (\rho \boldsymbol{u}) = 0$$

$$\frac{\partial (\rho \boldsymbol{u})}{\partial t} + \nabla \cdot (\rho \boldsymbol{u}\boldsymbol{u}) = -\nabla p + \nabla \cdot [\mu(\nabla \boldsymbol{u} + \nabla \boldsymbol{u}^T)] + \rho \boldsymbol{g} + \boldsymbol{F}$$

$$\frac{\partial}{\partial t}\alpha + \frac{\partial}{\partial x_i}(\alpha u_i) = 0$$

where ρ is the density, $\boldsymbol{u}$ is the velocity vector, μ is the kinematic viscosity of the lubricant, $\boldsymbol{g}$ is the gravitational acceleration and $\boldsymbol{F}$ represents the external forces. α is a scalar that represents the volume fraction of the one of the two phases in each computational cell. The averaged properties (ϕ)

Preprints (www.preprints.org) | NOT PEER-REVIEWED | Posted: 18 October 2019 doi:10.20944/preprints201910.0218.v1

of the mixture in each cell of the domain are calculated as an α-averaged value of the properties of air and lubricant.

$$\phi = \phi_{lub} \cdot \alpha + \phi_{air} \cdot (1 - \alpha)$$

3. Results

The main goal of the project was to study the effects of the geometrical simplifications on the lubricant distribution and the power losses. The sectorial simulations were performed on the VSC cluster [19] while the full simulation (#4) on a Deploy Linux LXD [20] Compute Node [21] backed by a Ceph storage cluster [22]. Table 5 summarizes the properties of the computational nodes.

Table 5. Hardware

Name	CPU x node	Ram x node
VSC	2xAMD Opteron Magny Cours 6132HE (8 Cores, 2.2GHz)	8x4Gb ECC DDR3
LXD	2xINTEL Xeon® E5-2680 (8 Cores, 3.5GHz)	12x32Gb ECC DIMMs

Figure 7 reports the predicted power losses of the different configurations. Despite the different geometries, mostly between #1 and #2 (ribs), the power losses result comparable. However, it is opinion of the authors that these results cannot be generalized to different rotational speeds. The rounding radii seem to not affect significantly the power dissipation. It can be observed that the regime condition (stabilization of the losses) is reached much faster in the simulation #1. The absence of ribs, in fact, promotes an easier lubricant flow in the axial direction.

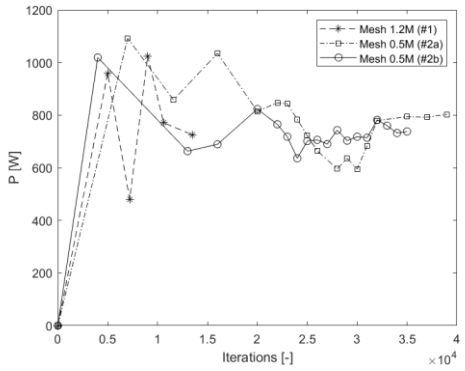

Figure 7. Power losses of the bearing.

While simplification #1 seems to significantly modify the physical problem producing meaningless results, figure 7 shows the effect of the rounding radii. On the left-hand side #2 is shown. The absence of the rounding radii on the external race causes a stagnation of the lubricant and a higher wetting of the outer radial surface of the cage. This impacts also on the wetting of the radial surface of the roller that results less lubricated in configuration #3.

Figure 9 highlights the differences induced by the relative position to the roller with respect to the gravitational acceleration. It appears how small differences in terms of oil distribution are present even if the structure of the bearing is axis-symmetric and the mesh is the same for each sector. The lower the position of the roller, the higher its lubrication.

Preprints (www.preprints.org) | NOT PEER-REVIEWED | Posted: 18 October 2019 doi:10.20944/preprints201910.0218.v1

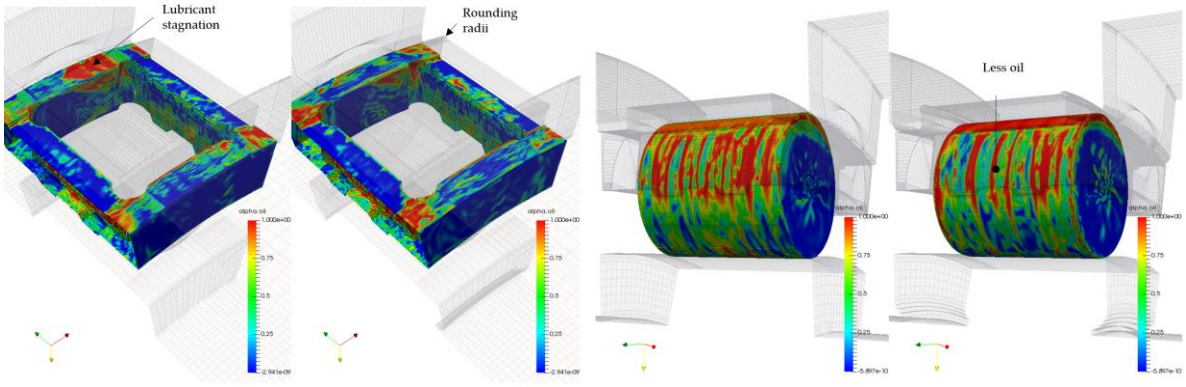

Figure 8. Effect of the rounding radii: wetted surfaces (contour of the volume fraction 0÷1) of cage and roller - models #2 (left) vs #3 (right).

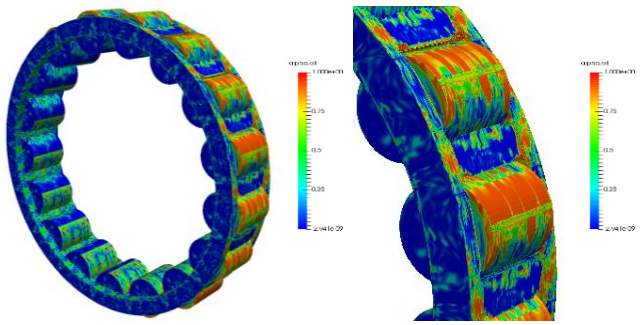

Figure 9. Effect of the gravitational force: wetted surfaces (contour of the volume fraction 0÷1) of cage and rollers - #4

3.1. Computational effort and scalability

The 7.3M- and the 1.2M-cells meshes (configuration #1) were used to assess the scalability of the numerical model on the number of processors. For the finer grid, simulations were performed on the VSC cluster using 64, 128 and 256 cores. Figure 10 (left) shows the good scalability of the results. The same was made for the 1.2M mesh. While the scalability seems to be linear up to 64 cores, the time required for the solution does not reduce significantly with 128 cores. With 256 cores, the computational effort even increases. This is due to the times required for the exchange of information between processors that become higher than the solution time itself. The perfect balance was found to be around 20k cells per core.

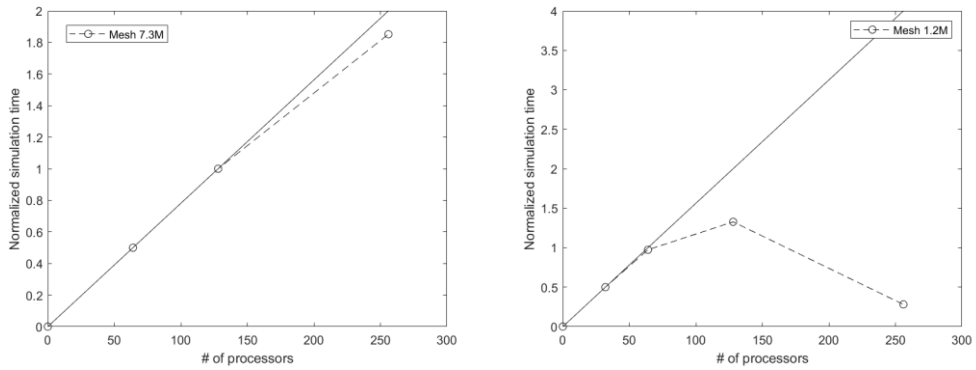

Figure 10. Scalability on number of processors (#1 - VSC)

5. Conclusions

OpenFoam® 4.1 with some specifically developed B.C. seems to be suitable for lubrication simulations. A sector of a Schaeffler NU222-E-XL-M1 bearing was modelled with hexahedral elements taking advantage of different meshing strategies. The studied geometrical simplifications seem to not significantly affect the power losses but unquestionably the lubricant distribution and lubrication of the different components. The presence of the rounding radii on the outer ring promotes the lubricant circulation reducing its stagnation between cage and rings. The components result less wetted.

The gravity seems to slightly affect the wetting of the rollers depending on their position along the circumference of the bearing.

The proposed meshing approaches enable different levels of geometrical complexity. The capability to create a 3D grid starting from a simple extrusion allows a much better control of the mesh quality that directly affects the convergence of the solution and, therefore, the computational effort required.

Scalability tests have shown, for 2 different grids, that an averaged number of cells per core of about 20k is the best balance between computational resources and computational effort (on the present hardware).

Funding: This research was funded by Schaeffler Technologies AG & Co. KG, grant number TN2369-C and TN2371-C.

Acknowledgments: The authors would thank Cristiano Cumer for the support with the LXD cluster.

Conflicts of Interest: authors declare no conflict of interest

References

[1] Z. Ji, M. Stanic, E. A. Hartono, and V. Chernoray, "Numerical simulations of oil flow inside a gearbox by Smoothed Particle Hydrodynamics (SPH) method," *Tribol. Int.*, vol. 127, pp. 47–58, 2018.

[2] F. Concli and C. Gorla, "Windage, churning and pocketing power losses of gears: different modeling approaches for different goals," *Forsch. im Ingenieurwesen/Engineering Res.*, vol. 80, no. 3–4, 2016.

[3] P. H. L. Groenenboom, M. Z. Mettichi, and Y. Gargouri, "Simulating Oil Flow for Gearbox Lubrication using Smoothed Particle Hydrodynamics," *Proc. Int. Conf. Gears 2015*, 2015.

[4] F. Concli and C. Gorla, "CFD simulation of power losses and lubricant flows in gearboxes," in *American Gear Manufacturers Association Fall Technical Meeting 2017*, 2017, vol. 2017-Janua.

[5] Ted Ørjan Kjellevik Gundersen, "Modelling of Rotating Turbulent Flows," NTNU, 2011.

[6] F. Concli, C. Gorla, A. D. Torre, and G. Montenegro, "Windage power losses of ordinary gears: Different CFD approaches aimed to the reduction of the computational effort," *Lubricants*, vol. 2, no. 4, pp. 162–176, 2014.

[7] M. Wang, X. Xu, X. Ren, C. Li, J. Chen, and X. Yang, "Mesh partitioning using matrix value approximations for parallel computational fluid dynamics simulations," *Adv. Mech. Eng.*, vol. 9, no. 11, 2017.

[8] F. Concli and C. Gorla, "Numerical modeling of the churning power losses in planetary gearboxes: An innovative partitioning-based meshing methodology for the application of a computational effort reduction strategy to complex gearbox configurations," *Lubr. Sci.*, 2017.

[9] C. J. Hwang and S. J. Wu, "Global and local remeshing algorithms for compressible flows," *J. Comput. Phys.*, vol. 102, no. 1, pp. 98–113, 1992.

[10] J. Zheng, J. Chen, Y. Zheng, Y. Yao, S. Li, and Z. Xiao, "An improved local remeshing algorithm for moving boundary problems," *Eng. Appl. Comput. Fluid Mech.*, vol. 10, no. 1, pp. 403–426, 2016.

[11] F. Concli, A. Della Torre, C. Gorla, and G. Montenegro, "A New Integrated Approach for the Prediction of the Load Independent Power Losses of Gears: Development of a Mesh-Handling Algorithm to Reduce the CFD Simulation Time," *Adv. Tribol.*, vol. 2016, 2016.

[12] F. Concli and C. Gorla, "Numerical modeling of the power losses in geared transmissions: Windage, churning and cavitation simulations with a new integrated approach that drastically reduces the computational effort," *Tribol. Int.*, vol. 103, 2016.

[13] J. M. Rubio, "Multidimensional simulations of external gear pumps," Politecnico di Milano, 2017.

[14] F. Concli, "Pressure distribution in small hydrodynamic journal bearings considering cavitation: a numerical approach based on the open-source CFD code OpenFOAMÂ®," *Lubr. Sci.*, vol. 28, no. 6, 2016.

[15] F. Concli and C. Gorla, "Analysis of the oil squeezing power losses of a spur gear pair by mean of CFD simulations," in *ASME 2012 11th Biennial Conference on Engineering Systems Design and Analysis, ESDA 2012*, 2012, vol. 2.

[16] F. Concli and C. Gorla, "Oil squeezing power losses in gears: A CFD analysis," in *WIT Transactions on Engineering Sciences*, 2012, vol. 74.

[17] "OpenFOAM User Guide." .

[18] "www.hpfem.jku.at/netgen/." .

[19] "http://vsc.ac.at/." .

[20] "https://linuxcontainers.org/." .

[21] "https://www.cisco.com/c/dam/en/us/products/collateral/servers-unified-computing/ucs-b-series-blade-servers/B200M3_SpecSheet.pdf." .

[22] "https://ceph.com." .